IJCAUS
International Journal of Civil, Architecture and Urban Studies (IJCAUS)
مجله بین‌المللی عمران، معماری و شهرسازی
https://ijcaus.ir
دوره 2 – شماره 2 (تابستان 1405) – صفحه 15 تا 30

Experimental and Numerical Study of Seismic Behavior of Reinforced Concrete Shear Walls with Steel Fibers under Cyclic Loading

Ali Masoumi[1], Seyed Amir Ehsan Mousavi[2]

1- PhD Student in Civil Engineering – Structural Engineering, Faculty of Engineering, University of Qom, Qom, Iran , ali.masoumi.civil.76@gmail.com

2- Undergraduate Student in Civil Engineering, Islamic Azad University, Qom Branch, Qom, Iran , ehsanmou2013@gmail.com

Abstract

Steel-fiber-reinforced concrete (SFRC) offers a mechanism for bridging cracks, restraining crack opening, and modifying damage localization in reinforced-concrete (RC) shear walls subjected to reversed cyclic loading. This manuscript combines a reproducible laboratory testing plan, an explicitly specified nonlinear finite-element framework, and a critical synthesis of verified studies published primarily between 2024 and 2026. A controlled wall matrix is developed around fiber volume fraction, wall aspect ratio, axial-load ratio, and boundary reinforcement, with a prescribed displacement history and harmonized response measures. Material characterization, instrument placement, inverse calibration, energy dissipation, equivalent viscous damping, stiffness degradation, and uncertainty analysis are defined sufficiently to guide implementation. Reported published findings consistently indicate improved cracking control and deformation capacity in several SFRC wall configurations; however, the magnitude of the gain depends on detailing, axial compression, geometry, fiber dispersion, and failure mode. The manuscript distinguishes literature evidence from hypothetical specimen specifications and illustrative mechanical calculations. No invented laboratory measurements, simulation outputs, or validation error statistics are represented as observed results. The proposed framework provides a transparent path to a future experimentally validated study and identifies the minimum evidence necessary to evaluate a fiber-related seismic benefit without conflating it with confinement or reinforcement changes.

Keywords: steel-fiber-reinforced concrete, reinforced concrete shear wall, cyclic loading, seismic resilience, nonlinear finite-element analysis, energy dissipation

1. Introduction

Structural shear walls provide a primary lateral-force-resisting mechanism in multistory RC buildings. During earthquake-induced reversals, their response reflects interacting flexure, web shear, axial compression, reinforcement yielding, bond deterioration, and concrete damage. Even when peak strength is sufficient, residual drift, boundary crushing, bar buckling, and shear sliding can undermine repairability. Consequently, evaluating seismic performance requires more than comparing peak base shear; deformation capacity, cyclic stability, stiffness and strength deterioration, dissipated energy, and residual displacement must also be considered [1–5].

Steel fibers are dispersed short reinforcements intended to transfer traction across developing cracks. Depending on fiber geometry and orientation, matrix strength, and bond, they can restrain crack widths and redistribute stresses after matrix cracking. These effects are particularly relevant for walls in which diagonal cracking, flexural hinge formation, or local crushing controls seismic deterioration. Nevertheless, fibers do not automatically replace distributed bars, boundary confinement, or anchorage detailing. A sound interpretation must separate the effect of the cementitious composite from that of conventional reinforcement and boundary-zone design [1–4, 6–9].

Recent studies have enriched this topic by testing SFRC walls with conventional or alternative reinforcement, walls featuring door openings, and steel-fiber composite systems [1–4, 10]. Related research examines repeated compression, flexural cyclic properties, interface shear, and composite wall modeling [11–18]. The collective evidence is informative yet difficult to combine quantitatively because programs differ in shear-span ratio, concrete grade, axial loading, fiber volume, reinforcement ratio, loading protocol, and how ultimate displacement is defined.

The central methodological challenge is therefore comparability. A wall with greater fiber dosage but higher confinement or lower axial force is not a clean fiber-only comparison. Similarly, a finite-element simulation may fit peak force while failing to reproduce pinching, unloading stiffness, crack concentration, or cyclic strength loss. This work addresses both concerns by specifying a factorial test program and a hierarchical calibration workflow that treats multiple response features as independent validation targets.

The title is retained to match the intended subject, but the present contribution is intentionally classified as a research-design and evidence-synthesis manuscript. It does not claim that the proposed specimens were cast, tested, or simulated. Observations in the Results section are attributable to published reports and are explicitly identified as such. All proposed dimensions, constitutive coefficients, and figures are design assumptions or illustrations to be verified in future work.

1.1 Research questions and working hypotheses

RQ1: Under identical reinforcement and axial force, does an increased steel-fiber fraction delay crack localization and improve the deformation attained before a prespecified loss of lateral strength? H1 predicts improved crack control and greater postpeak deformation up to a practical material-dependent dosage, without presupposing a monotonic increase in peak strength.

RQ2: Is the benefit more pronounced in shear-critical than flexure-dominated walls? H2 predicts interaction between fiber dosage and shear-span ratio, because bridging mechanisms intersect inclined tension cracks differently from flexural toe damage.

RQ3: Can an independently calibrated cyclic finite-element model reproduce envelope resistance, unloading stiffness, pinching, and energy dissipation within prespecified tolerances? H3 predicts that tensile softening calibration improves envelope accuracy but separate reinforcement–concrete bond treatment is required for robust hysteresis prediction.

RQ4: How do axial-load ratio and boundary detailing modify fiber effectiveness and limit states? H4 predicts that greater axial compression can enhance initial shear resistance while increasing sensitivity to compression damage and reducing stable ductility under certain configurations.

2. State of knowledge and research gap

2.1 Direct evidence from SFRC wall tests

Full-scale cyclic investigations of SFRC shear walls with CFRP longitudinal bars compared conventional RC, nonfiber CFRP-reinforced concrete, and SFRC/CFRP variants. The published abstract reports improved damage control, bearing capacity, ductility, energy dissipation, and slower stiffness degradation as fiber fraction increased [1]. This is strong evidence that fiber-related behavior is plausible, but because the reinforcement class is changed across some comparisons, it is not a pure measure of steel fibers in otherwise identical steel-reinforced walls.

Tests of shear walls combining steel strands in boundary elements and steel fibers in the wall demonstrated improved resilience and energy dissipation with fiber fraction [2]. The study suggests that boundary-region load transfer and fiber bridging interact. It cannot be reduced to a universal fiber-strength coefficient without conditioning on the steel-strand arrangement and the associated confinement or bond response.

In-plane cyclic tests reported in 2024 found restrained damage, enhanced deformation, and reduced degradation after shear cracking in SFRC walls [3]. That report compared an SFRC specimen with 0.30% wall reinforcement with an ordinary RC specimen with 1.13% reinforcement, underscoring a promising design possibility but also emphasizing the need to avoid interpreting unlike reinforcement layouts as a directly controlled fiber-only experiment.

Experimental SFRC walls featuring door openings exhibited sensitivity to the position of openings [4]. More recent hybrid steel–concrete wall tests likewise showed that continuous reinforcement and opening configuration substantially affect load paths [5]. Fibers are therefore best treated as a complement to deliberate force-flow detailing, not a substitute for continuity across vulnerable piers and coupling regions.

2.2 Evidence from complementary cyclic and material tests

Tests of SFRC under repeated compression have shown a more stable cyclic compressive response and less visible crushing under certain tested mixtures [11]. Material-level responses support selection of compression parameters for a constitutive model, but specimen-scale cycles do not capture boundary-bar instability or global wall shear transfer.

Beam-level cyclic experiments and nonlinear modeling demonstrate sensitivity of flexural toughness to fiber content, geometry, and constitutive idealization [12]. Interface shear-transfer research [13] additionally clarifies that roughness, clamping reinforcement, and fiber bridging compete in mobilizing transfer across cracks. The transfer of these findings to walls should remain conditional on crack angle, cyclic opening, confinement, and member size.

Concrete-filled steel-tube and composite-wall studies offer insight into boundary confinement, alternative connection detailing, and cyclic finite-element validation [14–19]. They are indirect comparators rather than interchangeable observations for ordinary reinforced-concrete SFRC walls, because their steel plates, tubes, or hybrid reinforcement provide distinct mechanical paths.

2.3 Limitations of the recent literature

The literature contains several confounding patterns: changes to fiber fraction are accompanied by changes in reinforcement type; axial load is not standardized; cyclic loading histories vary; damage is described qualitatively without uniform crack-width maps; and ductility ratios depend on the adopted yield-point convention. Data digitized from graphs additionally carry sampling uncertainty, especially around sharply pinched reversal loops.

A second gap concerns model identifiability. Increasing tensile fracture energy, changing bond-slip stiffness, or reducing damage-plasticity degradation can produce similar peak force but distinct physical behavior. Calibrating a model exclusively to a single backbone risks nonunique parameter sets. A robust design should constrain material-level responses before wall-level matching, then reserve at least one specimen or protocol for blinded validation.

A third gap concerns uncertainty. Steel-fiber orientation varies with casting flow, formwork, thickness, aggregate grading, and consolidation. Since fibers activate through bridging a crack plane, nominal volume fraction alone is incomplete; observed orientation and distribution should be quantified in sawn sections or by image analysis and included as uncertainty or covariates.

3. Materials and methods: proposed laboratory program

This section defines an executable future experimental program; none of the specimen specifications below are observed or tested data. All values are preliminary design targets requiring checks against the applicable local structural standard, laboratory capacity, and a pilot mixture study.

3.1 Geometry, factor selection, and specimens

A reference rectangular wall with clear height 1800 mm, length 1200 mm, and thickness 150 mm is proposed, with a stiff 450 mm-deep foundation block and a reinforced top beam. The corresponding nominal shear-span ratio is approximately 1.5 when the lateral actuator acts at the top beam centerline. Keep reinforcement constant among fiber-only comparisons: two curtains of web bars, closely confined boundary elements, and identical foundation anchorage. A second aspect-ratio group may be achieved by increasing shear span while holding wall section constant; such changes should be modeled as separate geometry strata rather than silently pooled.

ID	Fiber vol. (%)	Axial ratio target	Shear span/length	Study purpose
RC-0	0.0	0.10	1.5	Reference
SF-05	0.5	0.10	1.5	Dosage comparison
SF-10	1.0	0.10	1.5	Dosage comparison
SF-15	1.5	0.10	1.5	Dosage comparison
SF-10-A	1.0	0.20	1.5	Axial interaction
RC-S	0.0	0.10	1.0	Shear-critical reference
SF-S	1.0	0.10	1.0	Shear-critical fiber effect
RC-F	0.0	0.10	2.0	Flexural reference
SF-F	1.0	0.10	2.0	Flexural fiber effect

Table 1. Proposed experimental matrix (design assumptions, not completed tests).

At least two nominal replicates per condition would permit estimation of test-to-test scatter; if funding limits replicates, a targeted repeat of the control, optimum-dose, and shear-critical specimens has priority. Randomize casting order where feasible and document batch, ambient temperature, curing, and placement direction. The fiber-by-geometry interaction is best estimated only after verifying sufficient replicates and consistent control failure modes.

3.2 Materials, mixing, and characterization

Select a target 28-day mean compressive strength of approximately 40 MPa as a design starting point, without treating it as a tested value. Use a fixed water-to-binder ratio and aggregate grading across the fiber series, while adjusting a compatible superplasticizer only as required to maintain workable placement. Record changes to admixture content to avoid obscuring possible mixture effects. Straight or hooked-end fibers may be used, but the choice must be held constant across the primary matrix.

A provisional hooked-end steel fiber of length 35 mm, diameter 0.55 mm (aspect ratio about 64), and specified tensile strength of at least 1000 MPa can be selected based on availability and manufacturer certification. Fiber mass is determined from the nominal volume fraction times mixture volume and steel density; this calculation excludes any allowance for handling loss. Before casting walls, conduct trial batches to examine balling, segregation, workability loss, and fiber orientation near reinforcement congestion.

Characterize concrete compression, splitting tensile strength, elastic modulus, and flexural residual strengths using recognized current laboratory methods suited to the jurisdiction. Record specimen count, curing age, coefficient of variation, failure observations, and fiber distribution; supplement with notched-beam bending where a tensile stress–crack opening law is needed. Tensile postcracking input should be inferred from tests rather than fitted freely from the desired wall hysteresis.

Test longitudinal and transverse rebar coupons for yield strength, strain hardening, and elongation. Record reinforcing bar diameter, clear spacing, anchorage, splice locations, stirrup hook angles, and cover, since these details directly affect boundary crushing, confinement, and reinforcement slip.

3.3 Loading apparatus and cyclic displacement history

Anchor the foundation beam to the strong floor using pretensioned rods and monitor unintended foundation rotation. Apply constant axial compression through a vertically guided actuator or a low-friction load-transfer system while a horizontal servo-hydraulic actuator imposes reversed displacement at the top beam. The vertical system must permit lateral displacement without introducing uncontrolled moment or friction that would alter measured shear response.

Use displacement control with drift ratios of 0.05%, 0.10%, 0.20%, 0.30%, 0.50%, 0.75%, 1.0%, 1.5%, 2.0%, 2.5%, and 3.0%; apply two fully reversed cycles at each level, subject to safe termination criteria. Define drift as the corrected top lateral displacement divided by clear wall height. For research comparability, preserve the actual measured time history and cycle count rather than reporting only nominal target amplitudes.

Test termination should be predefined, such as a sustained loss to 80% of the maximum lateral resistance on the envelope, loss of axial-load stability, critical anchorage damage, or the actuator travel limit. The 80% threshold is an analysis convention, not a universally safe collapse criterion. Observe and photograph cracking at each amplitude, with mapped residual crack widths after unloading.

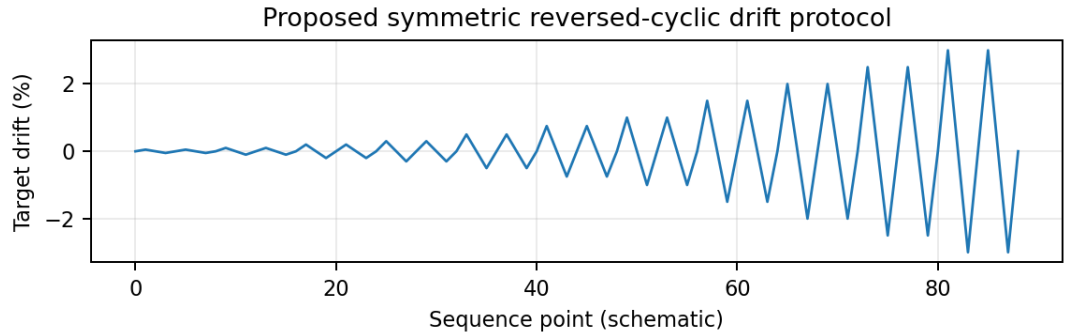


Figure 1. Proposed loading history; schematic points are not recorded actuator data.

3.4 Instrumentation and quality control

Synchronize actuator force, horizontal displacement, axial load, top-beam rotation, foundation movement, and local wall deformations at a sampling rate sufficient to capture hysteretic reversals. LVDTs at wall diagonals, vertical boundaries, top and bottom corners, and foundation interfaces permit separation of flexural, shear, and slip components. Distributed digital image correlation can map strain localization, provided lighting and calibration remain stable throughout the loading program.

Bonded strain gauges at selected longitudinal reinforcement, web bars, and boundary ties identify first yield and load redistribution. Photograph each wall at identical drift amplitudes and with visible scale references. For fiber walls, record crack width and spacing before and after each critical stage; use a predefined grid to minimize observational subjectivity. Test logs should include any actuator drift correction, temporary shutdown, instrument replacement, or axial force deviation.

Shear deformation can be approximated from diagonal-gauge compatibility, but this inversion becomes uncertain after wide cracking or out-of-plane motion. Report assumptions, missing channels, and any filtering applied. If out-of-plane displacements are not monitored, interpret flexure–shear decomposition as approximate rather than exact.

3.5 Response indices and formulas

Measure	Operational definition
Peak force	Maximum absolute lateral force in each loading direction; retain positive/negative values separately.
Initial stiffness	Slope of a documented low-amplitude secant or regression interval, not an unspecified visually selected tangent.
Secant stiffness	$K_i = \|F_i\|/\|\Delta_i\|$ at each designated drift and loading direction.
Energy dissipation	E_{cycle} = absolute area enclosed by the force–displacement loop using measured ordered points.
Equivalent damping	$\xi_{eq} = E_{cycle}/(4\pi E_s)$, with E_s the consistently defined maximum recoverable reference strain energy.
Ductility	$\mu = \Delta_u/\Delta_y$; specify yield definition and use Δ_u at 80% postpeak force only when reached.
Residual drift	Lateral displacement at zero shear following a completed displacement excursion.
Strength degradation	Ratio of second-cycle to first-cycle peak force at equal amplitude, reported by direction.
Pinching	Ratio of force near a fixed fraction of displacement on reloading to envelope force at that displacement.
Damage	Spatial distribution of cracks, crushing, spalling, bar instability, and sliding; not a single qualitative adjective.

Table 2. Harmonized cyclic-response measures required for reproducibility.

For pointwise energy integration, $E_{cycle} = |\Sigma\ [0.5(F_i+F_{(i+1)})(\Delta_{(i+1)}-\Delta_i)]|$ around a closed measured loop. Because pinched cycles and load offsets can distort an unclosed trace, connect the final point to the starting point only when justified; otherwise explicitly state the truncation convention. Determine displacement ductility independently for each loading direction before averaging; if a clear steel yield point is absent, use a defined equivalent-yield bilinear method and report its sensitivity.

4. Proposed nonlinear numerical model

4.1 Geometry, elements, reinforcement, and mesh

Use a three-dimensional continuum discretization for the concrete wall, boundary regions, foundation block, and top beam, with embedded truss or beam representations of reinforcement. Compare at least three mesh scales (for example, nominal solid-element edges of 75, 50, and 35 mm near anticipated cracking) and refine adaptively or locally where needed. Material regularization based on characteristic element length is essential if a softening law is used to mitigate mesh-dependent localization.

Prescribe axial load before initiating cyclic lateral displacements, maintain it throughout lateral loading, and model foundation restraints and actuator application locations consistently with the laboratory setup. If experimental base slip is substantial, include a foundation-contact or anchorage-slip representation; fully fixed roots can otherwise overestimate stiffness.

Fiber effects may be represented through a homogenized tensile residual stress–crack opening relation calibrated to material tests, rather than generating individual fibers at wall scale. This approach is efficient but assumes representative dispersion; it does not explicitly resolve orientation effects. A complementary stochastic orientation sensitivity can vary residual strength and fracture energy within measured distributions.

4.2 Constitutive assumptions and cyclic degradation

Concrete under compression can be modeled using a nonlinear hardening and softening stress–strain law with a damage or inelastic strain component; tension is described by an initial elastic branch followed by a crack-bridging residual response. Where concrete damaged plasticity is employed, the dilation angle, viscosity regularization, yield surface parameters, tensile stiffness recovery, and compressive stiffness recovery must be reported and tested for sensitivity.

Standard smeared-crack plasticity frameworks do not automatically reproduce all physical crack closure or reloading pinching phenomena. Rebar constitutive hysteresis, strain hardening, the Bauschinger effect, bond deterioration, and anchorage slip may be dominant in walls that develop diagonal sliding or large flexural cracks. Introduce interface elements or calibrated slip laws when measured evidence warrants them rather than compensating for absent slip by arbitrarily reducing concrete tensile strength.

The steel-fiber enhancement should primarily be assigned to postcracking tensile resistance, fracture energy, and—where directly demonstrated—compressive ductility; simply multiplying the concrete compressive strength by fiber dosage can misrepresent the physical mechanism. Residual tensile bridging functions should be calibrated from independent flexural or direct tensile tests and then carried into the structural-wall model with bounded uncertainty.

Under cyclic loading, distinguish irreversible deformation from recoverable stiffness reduction, and specify whether damage variables can recover upon crack closure. The numerical time increment and stabilization energy require convergence monitoring; excessive viscous stabilization may spuriously enlarge the predicted enclosed-loop area and apparent energy dissipation.

4.3 Identification, validation, and error metrics

Adopt three calibration tiers. Tier 1 fits constituent material tests, including concrete compressive curves, postcrack tensile response, and rebar hysteresis. Tier 2 fits a designated baseline RC wall to identify boundary conditions, bond parameters, and cyclic deterioration. Tier 3 uses the measured SFRC material response with as few further wall-specific adjustments as possible; reserve an SFRC specimen for independent prediction.

A successful model should reproduce at least four response families: (i) envelope peak and postpeak slope, (ii) unloading/reloading stiffness and pinching, (iii) integrated energy per drift level, and (iv) damage location/failure sequence. A peak-force match alone is insufficient. Preselect acceptance tolerances before calibration; for example, a target absolute peak-force error of less than 10% and energy discrepancy below 20% may be used as project goals, not as achieved metrics.

Quantify prediction error separately for loading directions: e_F = (F_model − F_test)/F_test, and analogous normalized metrics for drift capacity and cyclic energy. Aggregate using a transparent weighted objective and disclose weights; avoid tuning to make a single aggregate score appear favorable at the expense of an omitted failure mode. Bootstrap uncertainty or Bayesian posterior intervals can represent specimen-to-specimen and parameter variability when a sufficient dataset exists.

4.4 Parametric and uncertainty investigations

Parameter	Illustrative levels	Mechanism tested
Fiber fraction	0, 0.5, 1.0, 1.5%	Residual tensile bridging
Axial load ratio	0.05, 0.10, 0.20	Compression/shear interaction
Shear-span ratio	1.0, 1.5, 2.0	Shear–flexure competition
Boundary tie spacing	Baseline, 0.75× baseline	Confinement sensitivity
Tensile fracture energy	0.7×, 1.0×, 1.3×	Softening uncertainty
Bond-slip stiffness	0.5×, 1.0×, 2.0×	Pinching and sliding

Table 3. Proposed sensitivity matrix; all factor levels are hypothetical.

When interpreting any simulated trend, retain wall geometry and conventional reinforcement fixed within each contrast. Report failure-mode switching explicitly: a beneficial fiber addition may increase shear resistance while leaving the ultimate limit governed by boundary bar buckling. Hence a limited ductility improvement does not necessarily imply that crack bridging was ineffective; it may indicate that a different component controlled the system.

5. Results: evidence-based synthesis and analytical illustrations

No original wall tests or solver results were available for this manuscript. Accordingly, this section summarizes externally reported results and presents transparent analytical illustrations. The summary is not a pooled meta-analysis: numerical comparisons between unrelated papers are not treated as exchangeable experimental observations.

5.1 Summary of published investigations

Year	System	Evidence type	Result / interpretive scope
2024	SFRC walls with CFRP bars	Quasi-static full-scale wall tests	Improved reported damage response, ductility and energy [1]
2024	Steel-strand boundary SFRC walls	Cyclic tests of four configurations	Fiber dosage influenced energy and resilience [2]
2024	In-plane SFRC RC walls	Reversed in-plane cyclic tests	Damage mitigation and improved deformation [3]
2025	SFRC with door openings	Cyclic tests of opening layouts	Opening placement altered seismic response [4]
2026	Hybrid opening configurations	Cyclic tests of two hybrid walls	Reinforcement continuity and pier mechanism were decisive [5]
2024	SFRC / CFST composite walls	Low-cycle cracking assessment	Fiber / boundary components constrained cracks [6]

2025	SFRC plastic-hinge framework	Seismic design synthesis	Rotation-demand performance objectives proposed [7]
2025	SFRC cyclic compression	Repeated compression specimens	Reduced deterioration in tested mixtures [11]

Table 4. Selected published evidence; design differences preclude direct numerical pooling.

5.2 Crack control and failure localization

The most consistent qualitative mechanism across directly relevant literature is crack-width restraint rather than a universally fixed percentage gain in peak resistance. Cyclic observations of SFRC shear walls indicate reduced visible damage and more favorable deformation behavior in specific tested configurations [1–3, 6]. The role of opening layout in [4, 5] demonstrates why crack bridging can be insufficient when discontinuous reinforcement or a reduced pier width changes the dominant load path.

For the planned experiment, crack maps should therefore be analyzed together with the wall response instead of being attached only as post-failure photographs. Suggested quantitative endpoints include the number of cracks above a defined width, maximum residual crack width at 1% and 2% drift, total mapped crack length per wall area, and a localization index based on the proportion of measured crack opening concentrated in the most damaged region.

Orientation should be considered when interpreting contradictory specimens. Fibers aligned favorably with principal tensile stresses can provide a greater effective bridging stress than fibers predominantly parallel to the crack plane. Casting direction and local reinforcement congestion may generate strong spatial variations, so wall-scale averages conceal possible concentrated weak regions.

5.3 Envelope strength, stiffness, and deformation

Recent SFRC wall tests report improvements in strength, deformation, and slower stiffness loss for their tested combinations [1–3]. Yet these published findings are conditional: a program combining CFRP bars and fibers cannot isolate the same structural response as a conventional steel-bar wall with only the fiber fraction changed. Systematic reporting of matched-control contrasts is needed before generalized design multipliers can be proposed.

In the proposed analysis, positive and negative envelopes will be calculated separately to expose possible asymmetry from casting, bar anchorage, loading offsets, and prior damage. Key points should include first significant diagonal cracking, first reinforcement yield, maximum lateral force, the 80% postpeak force threshold, and the displacement at which stable axial support can no longer be retained.

It would be methodologically misleading to convert improved postcrack bending toughness at coupon or beam level directly into a proportional increase in wall ductility. Wall ductility depends on longitudinal reinforcement, confinement, shear demand, aspect ratio, and geometric boundary conditions. Measured improvements in one response measure do not imply identical improvements in others.

5.4 Energy dissipation and damping interpretation

Experimental publications indicate potential advantages of SFRC in energy absorption under reversals [1, 2], and cyclic material tests document enhanced toughness in specified loading scenarios [11, 12]. At wall level, greater enclosed-loop area can arise from broader hysteresis, larger attainable deformation, or higher peak force. These contributions should be separated by comparing energy at the same imposed drift and the cumulative energy reached before failure.

Equivalent viscous damping provides a convenient nondimensional comparison but depends on the reference elastic strain-energy convention and hysteretic-cycle selection. Two specimens with equal total cumulative energy can have different damping at a fixed drift because one survives more loading steps. Report both E_{cycle} and ξ_{eq}, and identify whether values refer to first or second cycles.

For an illustrative closed loop idealized as a symmetric parallelogram with force scale 200 kN, displacement scale 12 mm, and shape factor 0.55, the enclosed area would be $0.55 \times 4 \times 200 \times 12 = 2640$ kN·mm = 2.64 kJ. This is an arithmetic teaching example rather than a prediction or observation of an SFRC specimen; real loop integration must use recorded point sequences.

5.5 Illustrative normalized response curves

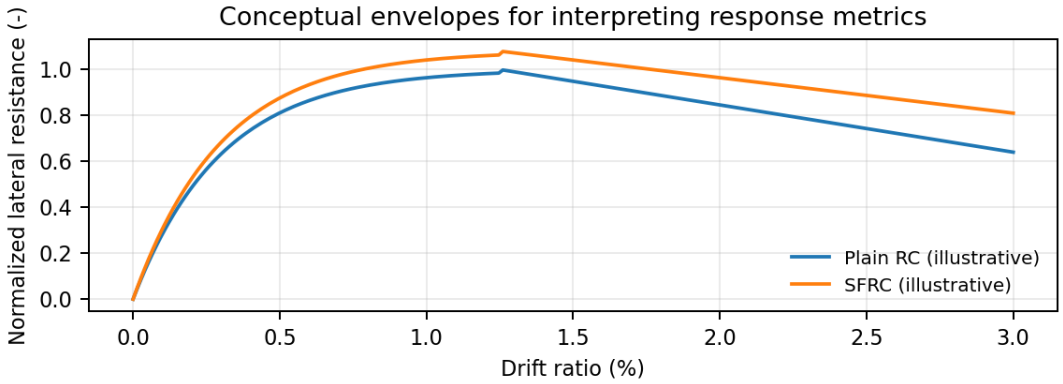


Figure 2. Fully illustrative curves; no fitted, measured, or simulated values are implied.

Figure 2 isolates the interpretation of postpeak retention: one curve can have only a modest increase in maximum force while retaining a greater fraction of resistance at large drift. The numeric coordinates are invented solely to explain metric extraction and must not be reported as research findings. A publishable version should replace this graphic with measured direction-specific envelopes and model predictions, both displaying confidence intervals where available.

5.6 Illustrative calculation of specimen material volumes

For the proposed rectangular wall web, the nominal concrete volume excluding the foundation and top beam is $1.8 \times 1.2 \times 0.15 = 0.324$ m³. At a nominal steel-fiber fraction of 1.0% and density 7850 kg/m³, the fiber mass would be approximately $0.01 \times 0.324 \times 7850 = 25.43$ kg. At 0.5% and 1.5% the corresponding masses would be 12.72 kg and 38.15 kg. These amounts

are design calculations, not batch records; actual total material quantities depend on boundary geometry, wastage, mix volume, and whether the boundary regions are fiber-reinforced.

Nominal Vf	Web volume (m^3)	Estimated fiber mass (kg)	Status
0.0%	0.324	0.00	Calculated
0.5%	0.324	12.72	Calculated
1.0%	0.324	25.43	Calculated
1.5%	0.324	38.15	Calculated

Table 5. Geometry-derived planning quantities; not physical test results.

6. Discussion

6.1 Mechanistic interpretation

The mechanisms most plausibly responsible for improved wall response are distributed bridging across multiple cracks, limited diagonal crack widening, delayed local crushing associated with altered stress concentrations, and improved postpeak stress redistribution. At increasing drift, however, fiber pull-out, rupture, or local absence may limit traction transfer. The gain is therefore expected to depend on the cracking regime rather than simply on the nominal addition rate.

In slender walls dominated by boundary flexural curvature, additional web bridging may reduce cracking without preventing reinforcement low-cycle fatigue or boundary crushing. Squat walls, by contrast, may offer greater scope for reducing dominant diagonal crack opening but can become susceptible to diagonal compression strut crushing or sliding. Both geometry classes are needed to distinguish structural advantage from altered failure mechanism.

SFRC should not be viewed as interchangeable with conventional transverse reinforcement. Closely spaced ties confine compressive zones and restrain buckling of longitudinal bars, functions that randomly oriented fibers cannot guarantee at a prescribed location. Conversely, uniformly distributed fibers may provide crack-scale transfer in regions where conventional bars are relatively widely spaced; their benefits are complementary.

6.2 Axial-load interaction and cyclic asymmetry

Constant compression stabilizes crack closure and may increase initial resistance, but elevated axial compression can promote toe crushing and accelerate loss of deformability once compression damage localizes. Experimental or analytical conclusions about fiber fraction are consequently incomplete without reporting the applied axial force and its normalization by concrete strength and effective area.

Positive/negative cycle asymmetry should not be eliminated by averaging too early. Wall construction tolerances, unequal bar anchorage, unintentional eccentricity, and nonuniform fibers can generate asymmetry even in nominally symmetric sections. Publishing signed cycle data aids verification and can reveal whether a model is merely matching a mean curve while missing one-direction degradation.

6.3 Numerical modeling and validation priorities

Wall-scale numerical results are not scientific validation unless they can be reproduced from named solver version, mesh definition, constitutive inputs, reinforcement layout, boundary conditions, time-step controls, and documented calibration data. Model reproducibility should also include the processing script that converts force–displacement history into hysteresis, envelopes, energy, and drift capacity.

The hierarchy of calibration protects against circular reasoning. If residual tensile capacity is tuned using the same SFRC wall response later offered as a successful prediction, the comparison describes fitting rather than validation. Independent material testing and a hold-out wall reduce such leakage. A parameter-identifiability analysis should be reported whenever several parameter combinations match the same peak strength.

Reference research on cyclic composite walls [14–19] shows that apparently similar global envelopes can accompany differing load-transfer arrangements. This observation motivates a failure-mechanism check: inspect crack concentration, rebar strains, anchorage slip, and local compressive damage together with global force–drift accuracy.

6.4 Practical engineering implications

For design, the strongest defensible conclusion from the current evidence is that fiber incorporation can improve aspects of seismic wall performance in appropriately detailed tested systems. The evidence does not yet justify a blanket reduction of code-required ties, webs, or boundary elements solely on the basis of a nominal fiber dosage.

When specifying SFRC, quality assurance should address batch uniformity, certified fiber properties, workability, placement orientation, and residual-strength acceptance. Performance specifications tied to measured residual flexural strength and crack width are more robust than dosage alone. Repairability and life-cycle value would require separate study of residual drift, crack sealing, corrosion risk, and repair intervention after cyclic damage.

An optimized design would compare increased material cost, labor and congestion benefits, constructability, and structural performance. Because these trade-offs depend on local pricing and code provisions, no universal optimal fiber fraction can be inferred from the reviewed evidence.

6.5 Strength of evidence and limitations

This manuscript is intentionally not an original experimental-results paper. It provides a fully articulated protocol and evidence synthesis but lacks new test datasets, solver execution, independent material calibration, uncertainty estimates from replicates, and structural-scale blind validation. Accordingly, it cannot substantiate numeric claims about the percentage gain in peak strength, ductility, or damping for the proposed wall series.

The cited sources include direct SFRC wall investigations and adjacent studies of fiber-reinforced materials, alternative reinforcement, or composite wall systems. Adjacent sources inform test setup and modeling mechanisms but should not be counted as independent demonstrations of SFRC effects in otherwise conventional RC shear walls. An eventual systematic review should include a preregistered search, exclusion criteria, risk-of-bias coding, and effect-size extraction before statistical pooling.

The proposed loading protocol is quasi-static and cannot represent all rate effects, cumulative duration, vertical earthquake accelerations, near-fault pulse characteristics, biaxial loading, or multi-story wall coupling. Additional dynamic studies will be necessary to extrapolate the results beyond the tested quasi-static regime.

7. Conclusions

1. The recent peer-reviewed literature supports a conditional, configuration-dependent ability of steel fibers to restrain cracking and improve deformation-related performance of several RC and composite shear wall configurations subjected to cyclic loading [1–6]. It does not establish a universal benefit independent of reinforcement, axial load, or geometry.

2. A valid fiber-effect comparison requires matched geometry, conventional reinforcement, compressive strength, applied axial compression, and loading history. The proposed nine-configuration matrix is a testable starting point; laboratory replication and pilot mixture evaluation are needed to determine feasible sample size and dosage.

3. Seismic evaluation should distinguish peak force, stiffness, strength degradation, ductility, first- and second-cycle energy, damping, residual drift, and repair-related crack damage. No single scalar metric adequately represents cyclic resilience.

4. A reproducible numerical study requires material-level identification of residual tensile behavior, explicit bond/anchorage decisions, mesh-objectivity checks, independent wall validation, and both global and local response comparisons. Matching only a peak lateral load is insufficient.

5. The principal research limitation is absence of newly measured wall and material datasets and of executed simulations. All program values and analytical examples in this paper are design assumptions or illustrations. The next step is to perform and archive the prescribed tests before making any original quantitative performance claims.

References

[1] Experimental and numerical investigation on seismic performance of SFRC shear walls with CFRP bars. (2024). Structures, 67, 106958. https://doi.org/10.1016/j.istruc.2024.106958

[2] Study on seismic performance of steel fiber reinforced concrete shear walls with hybrid steel strands and HRB400 bars in the boundary elements. (2024). Construction and Building Materials, 430, 136447. https://doi.org/10.1016/j.conbuildmat.2024.136447

[3] Experimental study on flexural properties of shear wall using steel fiber reinforced concrete under in-plane lateral force. (2024). Journal of Structural and Construction Engineering, 89(826), 1407. https://doi.org/10.3130/aijs.89.1407

[4] Seismic performance and shear capacity prediction of SFRC shear walls with different door openings. (2025). Structures, 72, 108198. https://doi.org/10.1016/j.istruc.2025.108198

[5] Influence of Opening Configuration on the Behavior of Hybrid Steel–Concrete Shear Walls with Steel-Fiber-Reinforced Concrete. (2026). Engineering Proceedings, 161(1), 12. https://doi.org/10.3390/engproc2026161012

[6] Crack characteristic and fractal analysis of SFRC shear wall with CFST columns under repeated low cycle load. (2024). Journal of Building Engineering, 97, 110978. https://doi.org/10.1016/j.jobe.2024.110978

[7] Seismic design method and application of steel fibre–reinforced concrete composite shear walls based on plastic hinge rotation demand. (2025). Journal of Building Engineering, 102, 111896. https://doi.org/10.1016/j.jobe.2025.111896

[8] The effects of steel fibers and boundary elements on the seismic behavior of high-strength concrete shear walls. (2023). Journal of Building Engineering. https://doi.org/10.1016/j.jobe.2023.106415

[9] Experimental study on seismic performance of squat RC shear walls reinforced with hybrid steel and GFRP rebars. (2024). Structures, 64, 106487. https://doi.org/10.1016/j.istruc.2024.106487

[10] Experimental Investigation of the In-Plane Cyclic Behavior of Hybrid GFRP-Steel Reinforced Squat Shear Walls. (2025). Engineering Research Journal, 184(2), 197–214. https://doi.org/10.21608/erj.2025.341951.1154

[11] Steel fibre reinforced concrete (SFRC) under repeated slow cyclic loading in compression – Experimental and theoretical studies. (2025). Structures, 78, 109303. https://doi.org/10.1016/j.istruc.2025.109303

[12] Experimental studies and non-linear finite element analysis of flexural behavior of steel fibre-reinforced concrete under monotonic and repeated cyclic loading. (2024). Discover Civil Engineering, 1, 61. https://doi.org/10.1007/s44290-024-00066-y

[13] Experimental Study of Interface Shear Transfer of Steel Fiber Reinforced Concrete Members. (2025). International Journal of Concrete Structures and Materials, 19, 28. https://doi.org/10.1186/s40069-024-00760-2

[14] Experimental and numerical cyclic response of mixed steel-concrete shear walls. (2024). Frontiers in Built Environment, 10, 1435899. https://doi.org/10.3389/fbuil.2024.1435899

[15] Experimentally validated numerical investigation on the behavior of composite shear walls subjected to cyclic loading. (2024). Engineering Science and Technology, 59, 101884. https://doi.org/10.1016/j.jestch.2024.101884

[16] Cyclic Behavior of Partially Prefabricated Steel Shape-Reinforced Concrete Composite Shear Walls: Experiments and Finite Element Analysis. (2024). Buildings, 14(7), 2208. https://doi.org/10.3390/buildings14072208

[17] Experimental and numerical investigation on seismic performance of an innovative steel-concrete composite shear wall. (2025). Journal of Building Engineering, 112075. https://doi.org/10.1016/j.jobe.2025.112075

[18] Performance evaluation of FRP-strengthened self-compacting concrete filled double-steel-plate composite shear walls: Experimental and numerical studies. (2025). Structures, 81, 110174. https://doi.org/10.1016/j.istruc.2025.110174

[19] Cyclic loading experiments on seismic performance of precast concrete superposed shear walls with CFST end columns. (2025). Journal of Building Engineering, 110527. https://doi.org/10.1016/j.jobe.2024.110527

[20] Evaluation of the seismic performance of novel bundled connections precast shear walls under cyclic loading. (2024). Structural Concrete. https://doi.org/10.1002/suco.202300809

[21] Shear–Flexural Performance of Steel Fiber-Reinforced Concrete Composite Beams: Experimental Investigation and Modeling. (2025). Materials, 18(18), 4322. https://doi.org/10.3390/ma18184322

[22] Cyclic compressive behavior and constitutive modeling of steel fiber–reinforced concrete after freeze–thaw cycles. (2026). Journal of Building Engineering, 121, 115671. https://doi.org/10.1016/j.jobe.2026.115671

[23] Reversed Cyclic Behavior of Carbon Nanofiber-Reinforced Concrete Shear Walls. (2024). Materials, 17(23), 5786. https://doi.org/10.3390/ma17235786

[24] Numerical investigation in the performance of welded multi-cavity double steel plate-concrete composite shear wall under cyclic loading. (2025). Journal of Building Engineering, 105, 112477. https://doi.org/10.1016/j.jobe.2025.112477

[25] Numerical prediction of seismic resistance and energy dissipation in CFRP-reinforced concrete shear walls under cyclic loading. (2026). Journal of Infrastructure Preservation and Resilience, 7, 2. https://doi.org/10.1186/s43065-025-00164-w

[26] Seismic Performance Test and Numerical Simulation of Steel Reinforced High-Strength Concrete Shear Walls. (2025). Structural Engineers, 41(3), 104–114. https://doi.org/10.15935/j.cnki.jggcs.202503.0011